

Nuclear imaging of bacterial infection- state of the art and future directions

Ilona Polvoy¹, Robert R. Flavell¹, Oren S. Rosenberg^{2*}, Michael A. Ohliger^{1,3*}, David M. Wilson^{1*}

¹Department of Radiology and Biomedical Imaging

University of California, San Francisco

San Francisco, CA 94158, USA

²Department of Medicine

University of California, San Francisco

San Francisco, CA 94158, USA

³Department of Radiology

Zuckerberg San Francisco General Hospital

San Francisco, CA 94110, USA

Contact information for the first author:

Ilona Polvoy, M.D.

Department of Radiology and Biomedical Imaging

University of California, San Francisco

185 Berry street

San Francisco, CA 94107, USA

Phone: (510) 680-6378

ilona.polvoy@ucsf.edu

***Correspondence and Reprint Request:**

David Wilson, M.D., Ph.D.

Department of Radiology and Biomedical Imaging

University of California, San Francisco

505 Parnassus Ave.

San Francisco, CA 94143, USA

Phone: (415) 353-1668

Fax: (415) 353-8593

david.m.wilson@ucsf.edu

Michael Ohliger, M.D., Ph.D.

Department of Radiology and Biomedical Imaging

University of California, San Francisco

1001 Potrero Ave. 1x55D

San Francisco, CA 94110, USA

Phone: (415) 206-8024

Fax: (415) 206-4004

michael.ohliger@ucsf.edu

Oren Rosenberg, M.D., Ph.D.

Department of Medicine

University of California, San Francisco

513 Parnassus Ave.

San Francisco, CA 94143, USA

Phone: (415) 514-0412

Fax: (415) 476-9364

oren.rosenberg@ucsf.edu

Running title: Nuclear imaging of bacterial infection

Keywords: infection, imaging, nuclear medicine, positron emission tomography, single photon emission computed tomography

Conflicts of Interest: The authors report no conflicts of interest relevant to this article.

ABSTRACT

Increased mortality rates from infectious diseases is a growing public health concern. Successful management of acute bacterial infections requires early diagnosis and treatment, which are not always easy to achieve. Structural imaging techniques such as computed tomography (CT) and magnetic resonance imaging (MRI) are often applied to this problem. However, these methods generally rely on secondary inflammatory changes and are frequently not specific to infection. The use of nuclear medicine (NM) techniques can add crucial complementary information, allowing visualization of infectious pathophysiology beyond morphologic imaging. This review will discuss the current structural and functional imaging techniques used for the diagnosis of bacterial infection and their roles in different clinical scenarios. We will also present several new radiotracers in development, with an emphasis on probes targeting bacteria-specific metabolism. As highlighted by the current COVID-19 epidemic, caused by the novel coronavirus SARS-CoV-2, similar thinking may apply in imaging viral pathogens; for this case prominent effects on host proteins most notably ACE2 might also provide worthwhile imaging targets.

LEARNING OBJECTIVES

On successful completion of this activity, participants should be able to (1) Learn the clinical justifications for using nuclear medicine techniques in imaging bacterial infections; (2) Understand the mechanism(s) of nuclear imaging methods used to detect bacterial infections; (3) Appreciate the bacterial-metabolism specific imaging techniques currently under development.

INTRODUCTION

Infectious diseases are a pressing public health concern. The rise of multidrug-resistant bacteria, especially in health care-associated infections, has resulted in increased mortality rates (1), despite the identification of new antimicrobial targets (2), and the focus on early diagnosis of disease. While this early diagnosis is crucial for patient management, it is not always easy to achieve. Although clinical history, physical examination, blood cultures or simple x-rays all assist in diagnosing infections, others require more complex imaging studies (3). One reason for this diagnostic difficulty is that infectious and inflammatory conditions have similar signs and symptoms, especially in patients with chronic infections, in patients with compromised immune systems, and in the elderly (4–6).

When more complex imaging is necessary, structural imaging techniques, such as computed tomography (CT), magnetic resonance imaging (MRI), and ultrasound are usually the next steps in the diagnostic approach. These techniques excel at identifying the presence of abnormal fluid, either within organs and other tissues, or forming discrete collections (i.e. abscesses). This abnormal distribution of fluid is related to increased vasodilation and vascular permeability resulting in tissue edema and “stranding” of normally fatty signal. However, these signs are non-specific and might appear in infection as well as in other inflammatory conditions (7,8). Additionally, anatomical changes that occur with chronic infection, such as bone destruction in osteomyelitis, weaken our ability to differentiate between active processes and treated disease (8,9).

Nuclear medicine (NM) techniques such as single positron emission tomography (SPECT) and positron emission tomography (PET) have also been applied to this problem. These methods allow visualization of infectious pathophysiology beyond structural imaging. The diagnostic accuracy of SPECT and PET is enhanced when structural modalities are used in tandem, and can pinpoint the exact location of the pathology with higher resolution compared to NM alone (10).

The proliferation of PET/CT, PET/MR and SPECT/CT dual imaging therefore has great potential to address the field of infectious disease imaging.

In this review we discuss the current imaging techniques for bacterial infection diagnosis, focusing on current NM methods, their limitations and how they are applied to common medical scenarios. We also provide a brief review of novel radiotracers currently in development, highlighting tracers that target bacterial metabolism.

IMAGING INFECTION – STATE OF THE ART

Imaging studies are frequently used to support the diagnosis of infection in acutely ill patients. Structural imaging studies include plain radiographs (X-rays), ultrasound, CT and MR. These methods can establish the presence of abnormal tissue or fluid collections that often accompany bacterial infection. For example, point-of-care ultrasound can be an effective tool for identifying the source of an infection as early as in the emergency department (11). Chest radiographs are used to detect consolidations, which are normally aerated portions of lung that are filled with liquid and tissue. Similarly, CT and MR can show the presence of inflammation and abscesses. These structural methods can be complemented by NM techniques (PET and SPECT) which represent a type of “molecular imaging,” whereby biochemical and physiologic abnormalities can be investigated. PET and SPECT are most helpful for equivocal cases, or for those where tissue sampling is difficult. In this section we summarize both structural techniques as well as current clinical NM methodologies (Figure 1).

Structural imaging techniques

The most commonly used noninvasive technique for the evaluation of tissue structure is the CT scan. This widely available examination produces high-resolution images and is considered the first-line choice in multiple clinical scenarios (12). However, CT has poor sensitivity

for detecting early infection due to the frequent absence of anatomical changes. Similarly, later in the disease, persistent anatomical abnormalities often mask chronic active infection. Moreover, ionizing radiation and the sensitivity of some patients to iodinated contrast also limits the use of CT (6,12,13). In contrast, MRI does not require ionizing radiation (12). It provides excellent soft tissue distinction even in the absence of contrast media (10). MRI is useful for the assessment of non-calcified tissues such as ligaments and viscera and is highly sensitive to tissue water content, allowing the diagnosis of inflammation, neoplasm, ischemia, and other abnormalities (14). However, MRI has low value in the evaluation of patients following surgery, and it can be potentially risky for patients with metallic implants or pacemakers (6,9).

Functional imaging techniques

In recent years there has been a growing interest in applying NM techniques (e.g. SPECT and PET) to the field of infectious disease (15,16), anticipating that metabolic abnormalities precede morphological changes identified using structural imaging (17,18). Moreover, the introduction of hybrid NM and structural technologies (i.e. PET/CT) has allowed better resolution for more precise localization of pathology making this approach highly appealing (19,20). In the next section, we will discuss the current clinically available applications of NM to infection. A summary of those techniques is shown in Table 1.

Bone Scintigraphy (BS). BS is a highly sensitive technique (20,21) that uses a labeled diphosphonate, most commonly, ^{99m}Tc -MDP, as a marker for active bone formation. Its uptake in pathological processes depends on two main factors, bone turnover and perfusion (18–20). These are abnormal in most pathological bone conditions, including infectious, traumatic, or neoplastic conditions, and therefore BS often requires a complementary imaging method to achieve diagnosis (20). BS is usually performed via one or less commonly, a triple-phase test, indicated by the suspected pathology. The single-phase study is performed a few hours post-injection and illustrates the metabolic activity of the bone itself. In contrast, the triple-phase bone

scan (TPBS) uses three different time points: (1) the “flow phase”, done immediately after the injection which demonstrates perfusion at the inflammation site (2), the “blood pool phase”, which shows the accumulation of blood in the soft and bone tissue caused by the blood flow and capillary dilatation and (3) the “bone uptake phase”, which illustrates the bone remodeling process after most of the soft tissue activity has washed-out (19). TPBS is especially valuable when trying to differentiate bone infection from other common clinical scenarios that can mimic its appearance. For example, soft tissue infection, unlike osteomyelitis, will not show tracer accumulation in the “bone uptake phase” (19).

Scintigraphy With Labeled Autologous White Blood Cells (WBC Scan). The WBC scan is a fairly common and sensitive technique that detects tagged WBC cells migrating to the site of infection through chemotaxis and diapedesis (3,22,23). It is considered the gold standard modality in many infectious scenarios, yet it has several drawbacks (23). The WBC scan can be a laborious and time-consuming procedure that exposes medical personal to blood products. It requires careful patient identification, and extraction and separation of WBCs from a whole-blood sample. Next, the WBCs undergo incubation with a radiotracer, usually ^{99m}Techneium or ¹¹¹indium, washing to remove any unbound radiotracer, and reinjecting cells into the patient prior to imaging (22,24). This examination is unsuitable for opportunistic or chronic infection due to the lymphocytic sensitivity to radiation as well as requiring the patient to have at least 2000 leukocytes (cells/μL), making it unfit for patients with granulocytopenia (22,24,25). Moreover, the phagocytosis of radiolabeled leukocytes by reticuloendothelial cells in the bone marrow can imitate normal hematopoiesis and therefore complicate the distinction of infected from reactive bone marrow. A possible solution is combining the WBC scan with an additional bone marrow (BM) scan. In this combined technique, an additional set of images with ^{99m}Tc-sulfur-colloid is acquired to indicate normal marrow distribution therefore improving the scan’s specificity (26).

⁶⁷Gallium-Citrate Scan. Although the ⁶⁷gallium-citrate scan has been used less frequently than in the past (15,16,25), it remains a good choice for several conditions, especially for spinal osteomyelitis (SOM) (25). It is used frequently when other modalities such as MRI or ¹⁸F-FDG-PET/CT are not available, and is particularly sensitive when combined with BS (4,13). Unlike the WBC scan, the ⁶⁷gallium-citrate scan does not require direct participation of immune cells, making it more suitable for immune-compromised patients (27). Gallium accumulates in sites of infection through several potential mechanisms. First, due to gallium's analogy to iron, it binds to transferrin and is recruited to inflammatory sites aided by increased vascular permeability and increased blood flow. Gallium may also bind to bacterial siderophores and activated lactoferrin in neutrophils, and is partially absorbed by macrophages (6,16,28).

FDG-Positron Emission Tomography. Established first in oncology, PET is currently the dominant modality in NM (15,17), with its most widely used radiotracer being the ¹⁸F-FDG, a glucose analog that accumulates in cells with high metabolic rates such as tumors or active inflammatory cells. The increased glycolysis of inflammatory cells in different stages of the infection - neutrophils, macrophages, and lymphocytes (17,18), makes this technique suitable for acute as well as chronic disease, although not specific to the presence of bacteria themselves (17). Moreover, the favorable pharmacokinetic characteristics of ¹⁸F-FDG allow perfusion in ischemic sites and promote imaging using a short post-injection delay of about 60 minutes (17,18). However, this exam is both expensive and not widely available (17), requiring the patient to adhere to a low-carbohydrate diet as well as fast in the 6 hour preceding the scan, avoid steroid treatment, regulate glucose levels, and abstain from high impact sports 24-hour prior to the examination (29). Differences in patient preparation therefore introduce considerable variability into the imaging outcome.

CLINICAL USES OF NUCLEAR MEDICINE IN IMAGING INFECTION

Imaging is essential in the evaluation of deeper infections, i.e. in the chest, abdomen or pelvis, or if the cause of infection is unknown. These scenarios frequently apply to sick inpatients, who are evaluated with a variety of structural and functional modalities including plain film, ultrasound, CT and MRI. Frequently structural imaging is enough to identify an abscess or other lesions. NM has an important and expanding role in three types of infection discussed here: (1) musculoskeletal infection, of joints, bone, and orthopedic hardware (2) cardiovascular infections, especially cardiac vegetations and infected prostheses and (3) infections whose source is not known, i.e. "fever of unknown origin".

Musculoskeletal infection - osteomyelitis

Osteomyelitis is an infection of bones and their surrounding structures, which is frequently caused by *S. aureus*. While this disease is typically disseminated hematogenously it can also spread locally, especially in the setting of trauma or surgery (9,18). Due to nonspecific symptoms, which might not include fever or pain, as well as variable physical examination and laboratory findings, delayed diagnosis is common (30). In the setting of prosthetic joint infection (PJI) this can lead to devastating results requiring removal of the infected prosthesis as the only treatment (31). In a patient with persistent symptoms and no neurologic deficit, the workup will begin with plain radiograph (X-rays). Yet due to its low sensitivity and specificity as well as late-appearing abnormalities, X-rays are used mostly to exclude other conditions (32). A more accurate tool is non-contrast MRI, since it can identify tissue changes within two days of infection onset, determine the involvement of bones and the surrounding tissues, and is sufficient for disease exclusion after only one week due to its high combined sensitivity and specificity and high negative predictive value (18,32,33). In most cases of suspected osteomyelitis, NM techniques are applied as complementary methods (20) due to their high sensitivity. However accurate diagnosis of osteomyelitis using existing tools is considered variable (32,34).

Peripheral Bone Infection. For acute infection of non-violated bones, TPBS, commonly enhanced by SPECT/CT is recommended (9,32). This highly sensitive technique is an excellent tool for excluding infection, especially when disease probability is low (32). However, once a bone had undergone intervention (e.g. trauma, surgery, metallic hardware), the already low specificity of TPBS decreases even further due to the bone remodeling process, making WBC/BM scan the test of choice for these situations (9,26,32). ¹⁸F-FDG-PET/CT is also less effective in violated bone, and is currently recommended mostly in cases of clinical suspicion for disseminated disease (32).

Spinal Osteomyelitis. In this entity, the ⁶⁷Gallium-citrate scan, frequently combined with a TPBS, can be a good alternative to MRI in SOM, with sensitivity and specificity over 90% (4). However, ¹⁸F-FDG-PET/CT has shown superiority to ⁶⁷gallium-citrate scan and BS in diagnosing SOM (35). Moreover, ¹⁸F-FDG-PET/CT has been shown to be superior to MRI for early (less than 2 weeks) and low grade infection and excellent for detecting chronic OM, with 96% sensitivity regardless of the disease phase (36). However, it lacks the ability to differentiate infection from sterile inflammation (37). WBC scan is not recommended for SOM due to its low sensitivity and the overlap of the imaging findings of SOM with other entities inciting marrow replacement (4,9).

Prosthetic joint infection. For PJI, TPBS has been frequently used, with the bone remodeling process creating several limitations in the first two years following surgery. In this early stage, either WBC scan or WBC/BM scan are recommended due to their high accuracy and ability to exclude the disease (17,34). However, in a recent study of chronic shoulder PJI, an extremely low sensitivity of 18% for WBC/BM scan was found, discouraging this recommendation (38). Figure 2 shows an example of WBC scan for PJI diagnosis in a 64 year-old (y/o) female after knee replacement.

While ^{18}F -FDG-PET/CT role for PJI is not fully clear (17) FDG-labelled-leucocytes PET/CT showed promising results when used in patients with painful joint arthroplasty, suggesting this method might be more specific than ^{18}F -FDG-PET/CT alone (39).

Cardiovascular system infection

NM, especially hybrid with structural imaging, has recently found a major role in CVS infection diagnosis. Although generally reserved for diagnostic failure of other imaging modalities, as well as for evaluation of complications and treatment response, the use of NM in cardiovascular disease is expanding (40). In 2015, radiolabeled WBC SPECT/CT and ^{18}F -FDG-PET/CT imaging were added to the infective endocarditis guidelines of the European Society of Cardiology as supplementary methods to assist in the workup of possible infective endocarditis according to DUKE's criteria in prosthetic valve endocarditis, as well as to detect extracardiac infectious foci and monitor treatment response (41). ^{18}F -FDG-PET/CT was able to diagnose about 40% of patients with systemic emboli regardless of symptomatology (40), however its 5 mm emboli threshold size as well as its nonspecific tracer uptake in an post-operative setting, may limit its use (41). In contrast, radiolabeled WBC SPECT/CT is less sensitive, yet more specific technique, even in a post-operative settings (42). A combination of the two modalities has shown a near 100% specificity highlighting the synergy of several imaging methods used in tandem (41,42). Figure 3 shows an example of ^{18}F -FDG-PET/CT in a 59 y/o patient with infective endocarditis.

Moreover, NM has been applied to less prevalent entities, such as vascular graft infection, in which CT angiography is commonly used. However, a recent meta-analysis showed WBC SPECT/CT had considerably higher pooled sensitivity and specificity compared ^{18}F -FDG-PET/CT and CT angiography suggesting this might be the most accurate modality for this entity (43).

Fever of unknown origin (FUO)

While FUO imaging workup usually begins with chest radiography and abdominal ultrasound (13), recent studies have shown the value of ^{18}F -FDG-PET/CT imaging and advised its completion in an earlier stage of disease evaluation (13,44). Historically, ^{67}Ga -citrate was the NM modality of choice in FUO (24); however, its low sensitivity, specificity and diagnostic yield have been suggested by a recent meta-analysis (45). Furthermore, a study that compared ^{67}Ga -citrate-SPECT/CT to ^{18}F -FDG-PET/CT showed higher sensitivity and clinical contribution for the latter (46).

Radiolabeled leukocytes are an alternative consideration. Although this method is considered accurate in patients where there is high suspicion of infection especially in the post-operative state(47), multiple studies which used leukocytes for FUO diagnosis showed low sensitivity and diagnostic yield, especially when compared to ^{18}F -FDG-PET/CT (13,45,48). While these and other studies show the superiority of ^{18}F -FDG-PET/CT in FUO diagnosis, ^{67}Ga -citrate and WBC scans are likely to be performed if ^{18}F -FDG-PET/CT is not available (13,48). Highlighting the ability of ^{18}F -FDG-PET/CT to localize in occult infection, Figure 4 shows an incidental finding of tonsillar abscess in a patient being evaluated for metastatic cancer.

NEWER APPROACHES TO MICROORGANISM-SPECIFIC IMAGING

A growing body of literature describing PET and SPECT imaging of infection demonstrates the increasing interest in this field. In addition to the clinically used tracers described above, multiple new methods have been reported to differentiate infection from sterile inflammation. Several of these radiotracers have targeted unique microbial pathways including bacteria-specific sugar transport, folic acid biosynthesis, iron accumulation, and cell wall components especially peptidoglycan (15,16,49). In this section we will provide a brief review on small molecules (<1000 Da) reported as promising bacterial-sensitive PET tracers in the last decade (Table 2). This review excludes several innovative protein and peptide-based radiotracer methods including radiolabeled antibodies.

Antibiotics

Many antibiotic and antifungal agents have been investigated as bacteria-specific diagnostic radiotracers, with ciprofloxacin being the most thoroughly studied. Although initially considered promising, ^{99m}Tc -ciprofloxacin showed inconsistent and unsatisfying results in several clinical trials suggesting low specificity for bacterial infection (50,51). A recent study speculated that this low performance might be related to the increase in drug-resistant bacteria (52). A more promising study was published recently by Sellmyer *et al.* who reported the PET analog bacterial dihydrofolate reductase inhibitor ^{18}F -fluoropropyl-trimethoprim (^{18}F -FPTMP), and showed that it could differentiate between infection, chemical inflammation and tumors in rodent models (Figure 5A) (53). Demonstrating its clinical promise, a dosimetry study of ^{11}C -trimethoprim was performed and showed that the absorbed radiation doses were well within safe limits for patients (54). Currently, this tracer is being evaluated further in clinical trials. Other fluoroquinolones, cephalosporins, and several anti-tuberculosis drugs have not yielded satisfactory imaging data (16,49,55).

Carbohydrates

One of the first carbohydrates to be explored as an infection-specific radiotracer was ^{18}F -FAG, a glucosamine analog, which could identify *E. coli* infection in rats with an approximately 2-fold calculated accumulation of the tracer in infected versus inflamed tissue (56). The bacterial universal hexose phosphate transporter has also been targeted. Mills *et al.* phosphorylated ^{18}F -FDG to produce ^{18}F -FDG-6-P, a substrate for this transporter, with promising *in vitro* results. However, while the tracer could differentiate infection from sterile inflammation in mice, the lower signal, and similar biodistribution to ^{18}F -FDG raised concerns regarding its clinical utility (57).

Several groups have targeted the maltodextrin transporter, a well-known system responsible for carbohydrate uptake in bacterial cells. ^{18}F -maltohexaose has shown promising preliminary results

in rats infected with *E. coli* when used to differentiate live from dead bacteria in the early stages of the bacterial infection (Figure 6A). It was both more sensitive and specific than ^{18}F -FDG showing a 7-fold increase in tracer accumulation in infected tissue compared to the sterile control, and sensitivity to drug-resistant bacteria (58). A similar approach was taken by Gowrishankar *et al.* using ^{18}F -fluoromaltose. This tracer showed an approximately 1.3-fold increase in tracer uptake in infection versus the sterile inflammation and high background noise (59). Later, ^{18}F -fluoromaltotriose, a second-generation tracer produced by the same group, showed better results accumulating in both *E. coli* and *Pseudomonas aeruginosa*, with a 3.4 fold higher tracer uptake in *E. coli* infected tissue versus sterile controls and an improved signal-to-noise ratio (Figure 6B) (60).

^{18}F -FDS, a fluorinated sorbitol analog, was first reported in 2008 as a potential cancer biomarker by Li *et al.* (61). This sugar alcohol is formed by a trivial chemical reduction of ^{18}F -FDG. The metabolism of this sugar in gram-negative bacteria was the premise of the 2014 Weinstein *et al.* study that showed a 7-fold increased uptake of ^{18}F -FDS in tissues infected with Enterobacteriaceae, including multidrug-resistant, compared to sterile inflammation in both immunocompetent and immunodeficient mice (62) (Figure 6C). Furthermore, the tracer showed dramatically decreased signal in mice infected with drug-susceptible and drug-resistant *E. coli* when they were treated with ceftriaxone. These results suggest that ^{18}F -FDS might not only help monitor antimicrobial therapy but also to identify resistant bacteria, allowing more accurate therapy in patients (62). Subsequently, several clinical trials have demonstrated ^{18}F -FDS safety in healthy human volunteers (63) as well as favorable renal kinetics (64).

Cofactor/DNA synthesis

The folate biosynthesis pathway has been targeted in antibiotic therapy most notably with trimethoprim/sulfamethoxazole therapy (inhibiting dihydrofolate reductase and dihydropteroate reductase respectively). Para-aminobenzoic acid (PABA) is a precursor of folic acid in bacteria

but not in mammalian cells, and its radiolabeled versions were studied both as ^{11}C -PABA (8) and ^{18}F -PABA (65). PABA showed incorporation in both gram-positive and gram-negative bacteria and the ability to identify infected tissue with an infection-to-inflammation ratio of 2.6 for ^{11}C -PABA and 7.95 for ^{18}F -PABA in *E. coli* and *S. aureus* infection (Figure 5B), respectively. Interestingly, when an unlabeled fluoro-PABA was added to the solution containing ^{18}F -PABA, as a mean to saturate the metabolic processes requiring it, the tracer uptake greatly increased, raising the infection-to-inflammation ratio to as high as 9.38 ± 2.43 . Furthermore, reduced uptake of ^{18}F -PABA in infected tissue treated with antibiotics was reported. This finding can potentially play a role in the identification of treatment response in the future (65). As described above, these folate precursors are closely related to the antibiotic-derived PET tracer targeting folate biosynthesis ^{18}F -FPTMP.

A radiotracer strategy more explicitly targeting bacterial DNA synthesis uses the nucleoside analog ^{124}I -FIAU, which is phosphorylated by thymidine kinases and subsequently trapped inside bacterial cells (16). Although promising in animal studies (16), this tracer showed inconclusive results in clinical trials. Even though ^{124}I -FIAU managed to diagnose musculoskeletal infection in a small group of patients, it later failed to do so when evaluating 22 patients with PJI and showed low specificity and poor image quality (66).

Iron transport and storage

While ^{67}Ga -citrate is a well-known and established SPECT radiotracer, its role in nuclear imaging has been decreasing. However, iron metabolism remains a focus in nuclear imaging research, with gallium (III) widely considered a surrogate for Fe (III). ^{68}Ga -citrate, a PET tracer with a 68 minute half-life, allows for same-day imaging and produces a higher image quality than its ^{67}Ga counterpart (67,68). Nevertheless, its diagnostic value has been controversial. While it has demonstrated high sensitivity in the diagnosis of discitis and osteomyelitis (69) distinguished septic from aseptic inflammation in prosthetic joint (70) and differentiated active from inactive

tuberculosis lesions (71), it failed to demonstrate an advantage over known modalities, such as labeled leukocytes and ^{18}F -FDG-PET in animal models. Moreover, it showed inferiority to ^{67}Ga -citrate in sixty patients with suspected bone or joint infection or FUO (68).

Siderophores, secreted iron chelators that are commonly used by both bacteria and fungi (49), have been extensively studied for bacteria- and fungus-specific detection. Petrik *et al.* have published several studies showing the potential of pathogen-specific siderophores for imaging studies. ^{68}Ga -TAFC and ^{68}Ga -FOX E were shown to be an effective tool for fungi imaging both *in vitro* and *in vivo* (72) and later, ^{68}Ga -pyoverdine-PAO1 a siderophore produced by *P. aeruginosa*, was shown to have an increased uptake in *Pseudomonas*-infected lung showing an improved distribution compared to ^{18}F -FDG and ^{68}Ga -citrate in animal models (73).

D-amino acids

Another approach targeting bacteria-specific structures uses substrates for the bacterial cell wall in particular peptidoglycan. Since mammalian cells generally use L-amino-acids as metabolic substrates, D-amino-acids are thought to be more specific to bacterial metabolism. Moreover, the fast incorporation of D-amino-acids into bacterial peptidoglycan in both gram-positive and gram-negative bacteria provides an appealing target for infection imaging. Neumann *et al.* showed a rapid accumulation of ^{11}C -D-Met in mice infected with *E. coli* and *S. aureus* without accumulation in the control sterile inflammation (37). Moreover, a recently published paper by Parker *et al.* showed a 3.5-fold higher accumulation of ^{11}C -D-ala in a mouse model of acute bacterial myositis compared to the sterile inflammation control, while ^{68}Ga -citrate showed only 2-fold higher accumulation in the same model. Furthermore, in a vertebral discitis-osteomyelitis model, ^{11}C -D-ala showed a 3.3-fold higher uptake relative to adjacent disc spaces and a 1.8-fold uptake in *P. aeruginosa* pneumonia relative to normal lung (74) (Figure 5C).

CONCLUSIONS

The limitations of current nuclear imaging methods to detect bacterial infection have motivated numerous new approaches targeting bacteria-specific proteins and metabolic pathways. Although the radiotracers studied are relatively unproven, success in this area may revolutionize the management of infectious diseases in clinical practice.

RADIOTRACERS ABBREVIATION LIST

Technetium-99m (^{99m}Tc)

Methylene diphosphonate (MDP)

2-deoxy-2- ^{18}F -fluoro-D-glucose (^{18}F -FDG)

^{18}F -fluoropropyl-trimethoprim (^{18}F -FPTMP)

2-deoxy-2- ^{18}F -fluoroacetamido-D-glucopyranose (^{18}F -FAG)

2-deoxy-2- ^{18}F -fluoro-D-glucose-6-phosphate (^{18}F -FDG-6-P)

6- ^{18}F -fluoromaltohexaose (^{18}F -maltohexaose)

4O(α -D-glucopyranosyl)-6-deoxy-6- ^{18}F -fluoro-D-glucopyranoside(^{18}F -fluoromaltose)

6-deoxy-6- ^{18}F -fluoro- α -D-glucopyranosyl-(1-4)-O- α -D-glucopyranosyl-(1-4)-O-D-glucopyranoside (^{18}F -fluoromaltotriose)

2-deoxy-2- ^{18}F -fluoro-sorbitol (^{18}F -FDS)

^{11}C -para-aminobenzoic acid (^{11}C -PABA)

2- ^{18}F -F-para-aminobenzoic acid (^{18}F -PABA)

Iodine-124-1-(2-deoxy-2-fluoro-1-D-arabinofuranosyl)-5-iodouracil (^{124}I -FIAU)

^{68}Ga -triacetylfusarinine C (^{68}Ga -TAFC)

^{68}Ga -ferrioxamine E (^{68}Ga -FOX E)

^{68}Ga -pyoverdine-PAO1 (^{68}Ga -PVD-PAO1)

D-methyl- ^{11}C -methionine – (^{11}C -D-Met)

D-3- ^{11}C -alanine – (^{11}C -D-Ala)

REFERENCES

1. Blair JMA, Webber MA, Baylay AJ, Ogbolu DO, Piddock LJ V. Molecular mechanisms of antibiotic resistance. *Nat Rev Microbiol*. 2014;13:42–51.
2. Lloyd DH. Alternatives to conventional antimicrobial drugs: a review of future prospects. *Vet Dermatol*. 2012;23:299-e60.
3. Meyer M, Testart N, Jreige M, et al. Diagnostic performance of PET or PET/CT using 18F-FDG labeled white blood cells in infectious diseases: a systematic review and a bivariate meta-analysis. *Diagnostics (Basel)*. 2019;9:60.
4. Berbari EF, Kanj SS, Kowalski TJ, et al. 2015 Infectious Diseases Society of America (IDSA) clinical practice guidelines for the diagnosis and treatment of native vertebral osteomyelitis in adults. *Clin Infect Dis*. 2015;61:e26-e46.
5. Tingstrom P, Milberg A, Sund-Levander M. Early nonspecific signs and symptoms of infection in institutionalized elderly persons: perceptions of nursing assistants. *Scand J Caring Sci*. 2010;24:24-31.
6. Xu T, Chen Y. Research progress of [68Ga]citrate PET's utility in infection and inflammation imaging: a review. *Mol Imaging Biol*. 2019;22(1):22-32.
7. Pober JS, Sessa WC. Inflammation and the blood microvascular system. *Cold Spring Harb Perspect Biol*. 2014;7:a016345.
8. Mutch CA, Ordonez AA, Qin H, et al. [11C]Para-aminobenzoic acid: a positron emission tomography tracer targeting bacteria-specific metabolism. *ACS Infect Dis*. 2018;4:1067-1072.
9. Lee YJ, Sadigh S, Mankad K, Kapse N, Rajeswaran G. The imaging of osteomyelitis. *Quant Imaging Med Surg*. 2016;6:184-198.

10. Khalil MM, Tremoleda JL, Bayomy TB, Gsell W. Molecular SPECT imaging: an overview. *Int J Mol Imaging*. 2011;2011:796025.
11. Cortellaro F, Ferrari L, Molteni F, et al. Accuracy of point of care ultrasound to identify the source of infection in septic patients: a prospective study. *Intern Emerg Med*. 2017;12:371-378.
12. Kumar R, Basu S, Torigian D, Anand V, Zhuang H, Alavi A. Role of modern imaging techniques for diagnosis of infection in the era of 18F-fluorodeoxyglucose positron emission tomography. *Clin Microbiol Rev*. 2008;21:209-224.
13. Mulders-Manders C, Simon A, Bleeker-Rovers C. Fever of unknown origin. *Clin Med*. 2015;15:280-284.
14. Berger A. Magnetic resonance imaging. *BMJ*. 2002;324:35.
15. Sethi I, Baum YS, Grady EE. Current status of molecular imaging of infection: a primer. *AJR Am J Roentgenol*. 2019;213:300-308.
16. Ordonez AA, Jain SK. Pathogen-specific bacterial imaging in nuclear medicine. *Semin Nucl Med*. 2018;48:182-194.
17. Vaidyanathan S, Patel CN, Scarsbrook AF, Chowdhury FU. FDG PET/CT in infection and inflammation—current and emerging clinical applications. *Clin Radiol*. 2015;70:787-800.
18. Palestro CJ. Radionuclide imaging of musculoskeletal infection: a review. *J Nucl Med*. 2016;57:1406-1412.
19. Dinh T, McWhorter N. Triple phase bone scan. StatPearls [Internet].
20. Van den Wyngaert T, Strobel K, Kampen WU, et al. The EANM practice guidelines for bone scintigraphy. *Eur J Nucl Med Mol Imaging*. 2016;43:1723-38.

21. Adams C, Banks KP. Bone scan. StatPearls [Internet].
22. Roca M, de Vries EFJ, Jamar F, Israel O, Signore A. Guidelines for the labelling of leucocytes with (111)In-oxine. Inflammation/infection taskgroup of the european association of nuclear medicine. *Eur J Nucl Med Mol Imaging*. 2010;37:835-841.
23. Auletta S, Riolo D, Varani M, Lauri C, Galli F, Signore A. Labelling and clinical performance of human leukocytes labelled with 99mTc-HMPAO using Leukokit® with Gelofusine versus Leukokit® with HES as sedimentation agent. *Contrast Media Mol Imaging*. 2019;2019:4368342.
24. Censullo A, Vijayan T. Using nuclear medicine imaging wisely in diagnosing infectious diseases. *Open forum Infect Dis*. 2017;4:ofx011.
25. Palestro CJ. Radionuclide imaging of osteomyelitis. *Semin Nucl Med*. 2015;45:32-46.
26. Palestro CJ, Love C, Tronco GG, Tomas MB, Rini JN. Combined labeled leukocyte and technetium 99m sulfur colloid bone marrow imaging for diagnosing musculoskeletal infection. *Radiographics*. 2006;26:859-870.
27. Palestro CJ. The current role of gallium imaging in infection. *Semin Nucl Med*. 1994;24:128-141.
28. Palestro CJ. The current role of gallium imaging in infection. *Semin Nucl Med*. 1994;24:128-141.
29. Surasi DS, Bhambhani P, Baldwin JA, Almodovar SE, O'Malley JP. 18F-FDG PET and PET/CT patient preparation: a review of the literature. *J Nucl Med Technol*. 2014;42:5-13.
30. Zimmerli W. Clinical practice. Vertebral osteomyelitis. *N Engl J Med*. 2010;362:1022-1029.
31. Tande AJ, Patel R. Prosthetic joint infection. *Clin Microbiol Rev*. 2014;27:302-345.

32. Glaudemans AWJM, Jutte PC, Cataldo MA, et al. Consensus document for the diagnosis of peripheral bone infection in adults: a joint paper by the EANM, EBJIS, and ESR (with ESCMID endorsement). *Eur J Nucl Med Mol Imaging*. 2019;46:957-970.
33. Momodu II, Savaliya V. Osteomyelitis. StatPearls [Internet].
34. Signore A, Sconfienza LM, Borens O, et al. Consensus document for the diagnosis of prosthetic joint infections: a joint paper by the EANM, EBJIS, and ESR (with ESCMID endorsement). *Eur J Nucl Med Mol Imaging*. 2019;46:971-988.
35. Fuster D, Solà O, Soriano A, et al. A prospective study comparing whole-body FDG PET/CT to combined planar bone scan with ⁶⁷Ga SPECT/ct in the diagnosis of spondylodiskitis. *Clin Nucl Med*. 2012;37:827-832.
36. Smids C, Kouijzer IJE, Vos FJ, et al. A comparison of the diagnostic value of MRI and ¹⁸F-FDG-PET/CT in suspected spondylodiscitis. *Infection*. 2017;45:41-49.
37. Neumann KD, Villanueva-Meyer JE, Mutch CA, et al. Imaging active infection in vivo using d-amino acid derived pet radiotracers. *Sci Rep*. 2017;7:7903.
38. Falstie-Jensen T, Daugaard H, Soballe K, Ovesen J, Arveschoug AK, Lange J. Labeled white blood cell/bone marrow single-photon emission computed tomography with computed tomography fails in diagnosing chronic periprosthetic shoulder joint infection. *J Shoulder Elb Surg*. 2019;28:1040-1048.
39. Aksoy SY, Asa S, Ozhan M, et al. FDG and FDG-labelled leucocyte PET/CT in the imaging of prosthetic joint infection. *Eur J Nucl Med Mol Imaging*. 2014;41:556-564.
40. Habib G, Erba PA, Lung B et al. Clinical presentation, aetiology and outcome of infective endocarditis. Results of the ESC-EORP EURO-ENDO (European infective endocarditis) registry: a prospective cohort study. *Eur Heart J*. 2019;40:3222-3232.

41. Habib G, Lancellotti P, Antunes MJ, et al. 2015 ESC guidelines for the management of infective endocarditis: the task force for the management of infective endocarditis of the European Society of Cardiology (ESC). *Eur Heart J*. 2015;36:3075-3128.
42. Rouzet F, Chequer R, Benali K, et al. Respective performance of 18F-FDG PET and radiolabeled leukocyte scintigraphy for the diagnosis of prosthetic valve endocarditis. *J Nucl Med*. 2014;55:1980-1985.
43. Reinders Folmer EI, Von Meijenfeldt GCI, Van der Laan MJ, et al. Diagnostic Imaging in Vascular Graft Infection: A Systematic Review and Meta-Analysis. *Eur J Vasc Endovasc Surg*. 2018;56:719-729.
44. Kouijzer IJE, Mulders-Manders CM, Bleeker-Rovers CP, Oyen WJG. Fever of unknown origin: the value of FDG-PET/CT. *Semin Nucl Med*. 2018;48:100-107.
45. Takeuchi M, Dahabreh IJ, Nihashi T, Iwata M, Varghese GM, Terasawa T. Nuclear imaging for classic fever of unknown origin: meta-analysis. *J Nucl Med*. 2016;57:1913-1919.
46. Hung B-T, Wang P-W, Su Y-J, et al. The efficacy of 18F-FDG PET/CT and 67Ga SPECT/CT in diagnosing fever of unknown origin. *Int J Infect Dis*. 2017;62:10-17.
47. Signore A, Jamar F, Israel O, Buscombe J, Martin-Comin J, Lazzeri E. Clinical indications, image acquisition and data interpretation for white blood cells and anti-granulocyte monoclonal antibody scintigraphy: an EANM procedural guideline. *Eur J Nucl Med Mol Imaging*. 2018;45:1816-1831.
48. Dibble EH, Yoo DC, Baird GL, Noto RB. FDG PET/CT of infection: should it replace labeled leukocyte scintigraphy of inpatients? *AJR Am J Roentgenol*. 2019;213:1358-1365.

49. Welling MM, Hensbergen AW, Bunschoten A, Velders AH, Roestenberg M, van Leeuwen FWB. An update on radiotracer development for molecular imaging of bacterial infections. *Clin Transl Imaging*. 2019;7:105-124.
50. Sarda L, Crémieux A-C, Lebellec Y, et al. Inability of ^{99m}Tc-ciprofloxacin scintigraphy to discriminate between septic and sterile osteoarticular diseases. *J Nucl Med*. 2003;44:920-926.
51. Dumarey N, Blocklet D, Appelboom T, Tant L, Schoutens A. Infecton is not specific for bacterial osteo-articular infective pathology. *Eur J Nucl Med Mol Imaging*. 2002;29:530-535.
52. Naqvi SAR, Roohi S, Sabir H, Shahzad SA, Aziz A, Rasheed R. Susceptibility of ^{99m}Tc-Ciprofloxacin for common infection causing bacterial strains isolated from clinical samples: an in vitro and in vivo study. *Appl Biochem Biotechnol*. 2019;188:424-435.
53. Sellmyer MA, Lee I, Hou C, et al. Bacterial infection imaging with [(18F)]fluoropropyl-trimethoprim. *Proc Natl Acad Sci U S A*. 2017;114:8372-8377.
54. Doot R, Young A, Schubert E, et al. First-in-human biodistribution and dosimetry of [11C] trimethoprim. *J Nucl Med*. 2019;60:1642.
55. Zhang Z, Ordonez AA, Smith-Jones P, et al. The biodistribution of 5-[18F] fluoropyrazinamide in Mycobacterium tuberculosis-infected mice determined by positron emission tomography. *PLoS One*. 2017;12:e0170871.
56. Martínez ME, Kiyono Y, Noriki S, et al. New radiosynthesis of 2-deoxy-2-[18F] fluoroacetamido-D-glucopyranose and its evaluation as a bacterial infections imaging agent. *Nucl Med Biol*. 2011;38:807-817.
57. Mills B, Awais RO, Luckett J, et al. [(18F)]FDG-6-P as a novel in vivo tool for imaging

- staphylococcal infections. *EJNMMI Res.* 2015;5:13.
58. Ning X, Seo W, Lee S, et al. PET imaging of bacterial infections with fluorine-18-labeled maltohexaose. *Angew Chem Int Ed Engl.* 2014;53:14096-14101.
 59. Gowrishankar G, Namavari M, Jouannot EB, et al. Investigation of 6-[¹⁸F]-fluoromaltose as a novel PET tracer for imaging bacterial infection. *PLoS One.* 2014;9:e107951.
 60. Gowrishankar G, Hardy J, Wardak M, et al. Specific imaging of bacterial infection using 6''-(¹⁸F)-fluoromaltotriose: a second-generation PET tracer targeting the maltodextrin transporter in bacteria. *J Nucl Med.* 2017;58:1679-1684.
 61. Li Z-B, Wu Z, Cao Q, et al. The synthesis of ¹⁸F-FDS and its potential application in molecular imaging. *Mol imaging Biol.* 2008;10:92-98.
 62. Weinstein EA, Ordonez AA, DeMarco VP, et al. Imaging enterobacteriaceae infection in vivo with ¹⁸F-fluorodeoxysorbitol positron emission tomography. *Sci Transl Med.* 2014;6:259ra146.
 63. Zhu W, Yao S, Xing H, et al. Biodistribution and radiation dosimetry of the enterobacteriaceae-specific imaging probe [(¹⁸F)fluorodeoxysorbitol determined by PET/CT in healthy human volunteers. *Mol imaging Biol.* 2016;18:782-787.
 64. Werner RA, Ordonez AA, Sanchez-Bautista J, et al. Novel functional renal PET imaging with ¹⁸F-FDS in human subjects. *Clin Nucl Med.* 2019;44:410-411.
 65. Zhang Z, Ordonez AA, Wang H, et al. Positron emission tomography imaging with 2-[(¹⁸F)f-p-aminobenzoic acid detects staphylococcus aureus infections and monitors drug response. *ACS Infect Dis.* 2018;4:1635-1644.
 66. Zhang XM, Zhang HH, McLeroth P, et al. [¹²⁴I]FIAU: Human dosimetry and infection imaging in patients with suspected prosthetic joint infection. *Nucl Med Biol.* 2016;43:273-

279.

67. Morgat C, Hindié E, Mishra AK, Allard M, Fernandez P. Gallium-68: chemistry and radiolabeled peptides exploring different oncogenic pathways. *Cancer Biother Radiopharm.* 2013;28:85-97.
68. Segard T, Morandea LMJA, Dunne ML, et al. Comparison between Gallium-68 citrate PET-CT and gallium-67 citrate scintigraphy for infection imaging. *Intern Med J.* 2019;49:1016-1022.
69. Nanni C, Errani C, Boriani L, et al. 68Ga-citrate PET/CT for evaluating patients with infections of the bone: preliminary results. *J Nucl Med.* 2010;51:1932-1936.
70. Tseng J-R, Chang Y-H, Yang L-Y, et al. Potential usefulness of (68)Ga-citrate PET/CT in detecting infected lower limb prostheses. *EJNMMI Res.* 2019;9:2.
71. Vorster M, Maes A, van de Wiele C, Sathekge M. 68Ga-citrate PET/CT in tuberculosis: a pilot study. *Q J Nucl Med Mol Imaging.* 2019;63:48-55.
72. Petrik M, Haas H, Laverman P, et al. 68Ga-triacetylfusarinine C and 68Ga-ferrioxamine E for aspergillus infection imaging: uptake specificity in various microorganisms. *Mol Imaging Biol.* 2014;16:102-108.
73. Petrik M, Umlafova E, Raclavsky V, et al. Imaging of Pseudomonas aeruginosa infection with Ga-68 labelled pyoverdine for positron emission tomography. *Sci Rep.* 2018;8:15698.
74. Parker MFL, Luu JM, Schulte B, et al. Sensing living bacteria in vivo using d-alanine-derived 11C radiotracers. *ACS Cent Sci.* 2020;6:155-165.
75. Yang R-H, Lee T-H, Chu Y-K. Unexpected thoracic endograft infection following a colorectal procedure. *Nucl Med Biomed Imaging.* 2016;1:7-9.

76. Truluck CA. Nuclear medicine technology: Inflammation and infection imaging. *J Radiol Nurs.* 2007;26:77-85.
77. American College of Radiology S for PR. ACR–SPR practice parameter for the performance of scintigraphy for inflammation and infection. 2018;1076:1-10.
78. Bartel TB, Kuruva M, Gnanasegaran G, et al. SNMMI procedure standard for bone scintigraphy 4.0. *J Nucl Med Technol.* 2018;46:398-404.

FIGURES

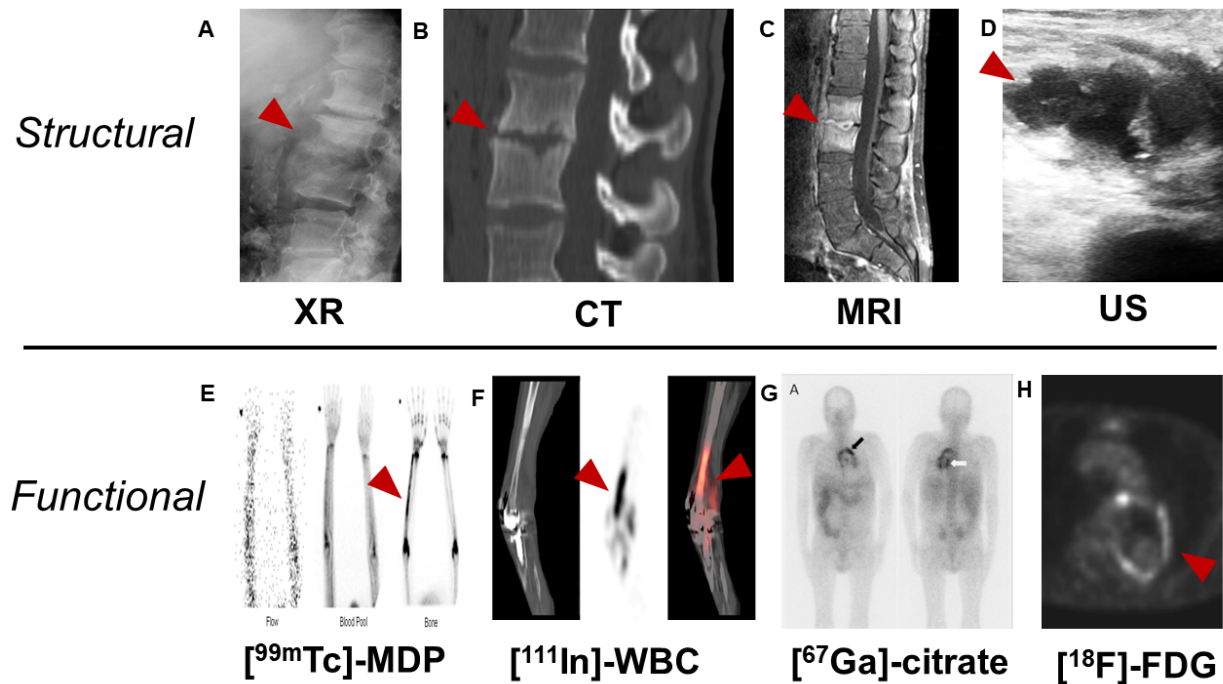


Figure 1: Examples of structural and functional imaging used in the diagnosis of infection. (A) Plain radiography of a 55 y/o male with DOM following corpectomy; (B+C) CT and MRI of a 23 y/o male with chronic DOM; (D) US of an 4 y/o male with perforated appendicitis and associated abscess; (E) ^{99m}Tc -MDP Bone scan of Right ulnar OM. From: Palestro *et al.* (25); (F) ^{111}In -WBC SPECT/CT of Infected right knee arthroplasty. From: Palestro *et al.* (25) (G) ^{67}Ga -citrate scan of a 61 y/o man with IVG of the aortic arch From: Yang, Lee, and Chu n.d. (75). (H) ^{18}F -FDG/PET of a 66 y/o male with infected thoracic aorta endograft.

*y/o – year old, DOM-discitis-osteomyelitis, IVG- infected endovascular graft

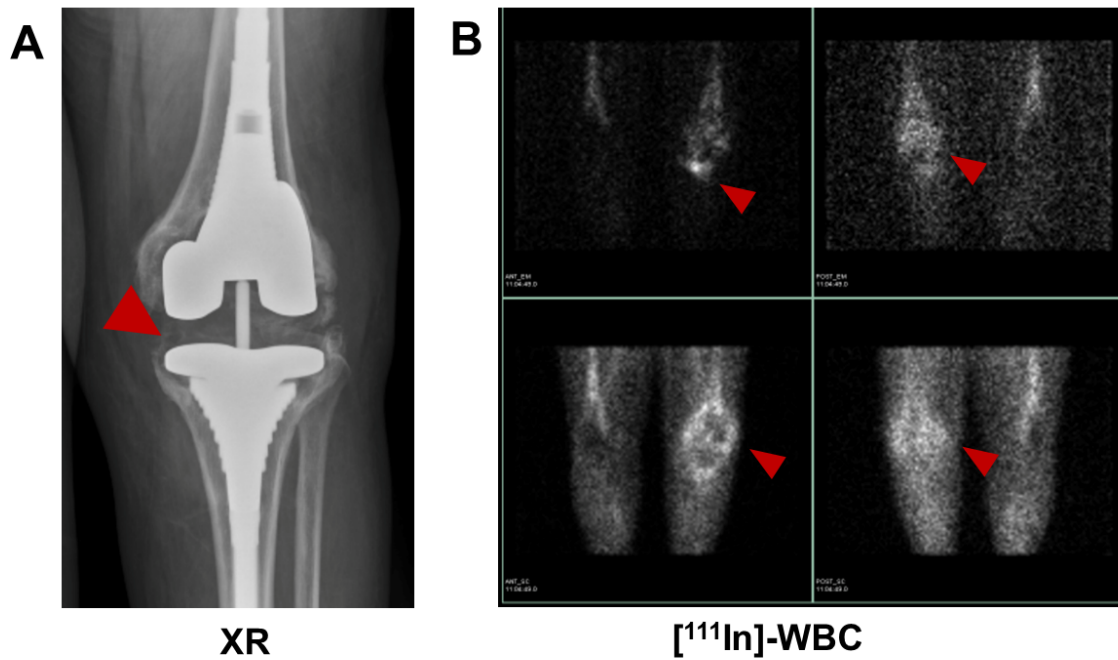


Figure 2: 64 y/o female with knee replacement and periprosthetic osteomyelitis as depicted via (A) plain radiography and (B) radiolabeled ¹¹¹In-leukocyte imaging (top row) demonstrates uptake brightest at the medial aspect of the tibial plateau. ^{99m}Tc-sulfur colloid imaging (bottom row) demonstrates no corresponding uptake in the region of the medial tibial plateau. Therefore, the findings are consistent with osteomyelitis.

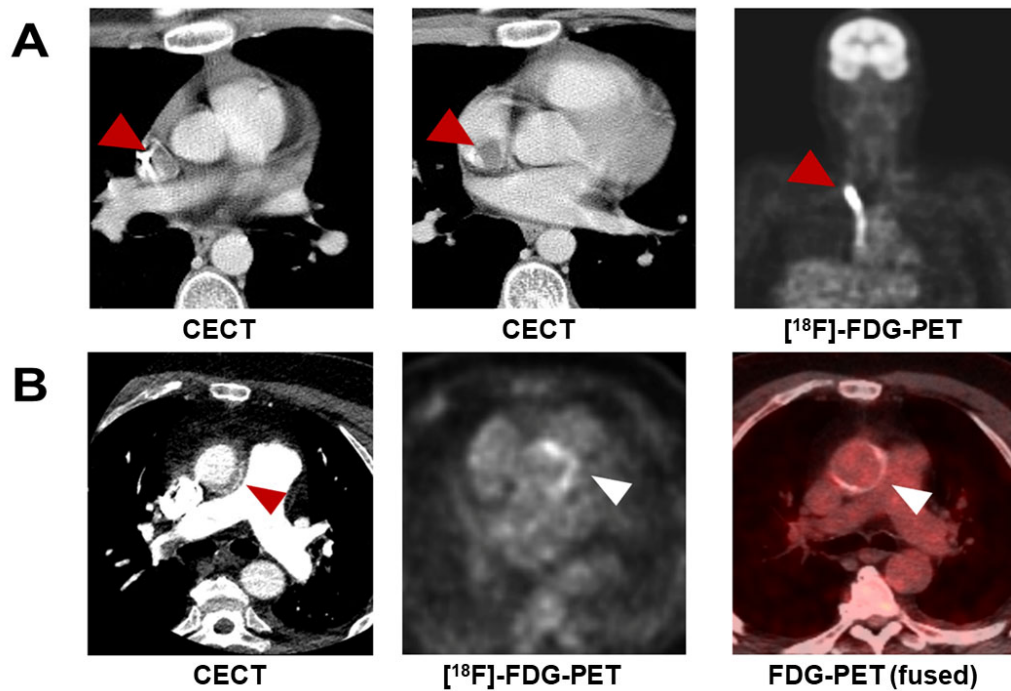


Figure 3: Examples of ^{18}F -FDG-PET in cardiovascular disease. (A) 17 y/o male with non-Hodgkin's lymphoma, found to have catheter-associated thrombus consistent with infection, with red arrow indicating increased FDG uptake in and around the catheter; (B) 59 y/o man with aortic valve prosthesis infection caused by *E. faecalis*; required surgical replacement, with white arrow indicating increased FDG uptake by the valve.

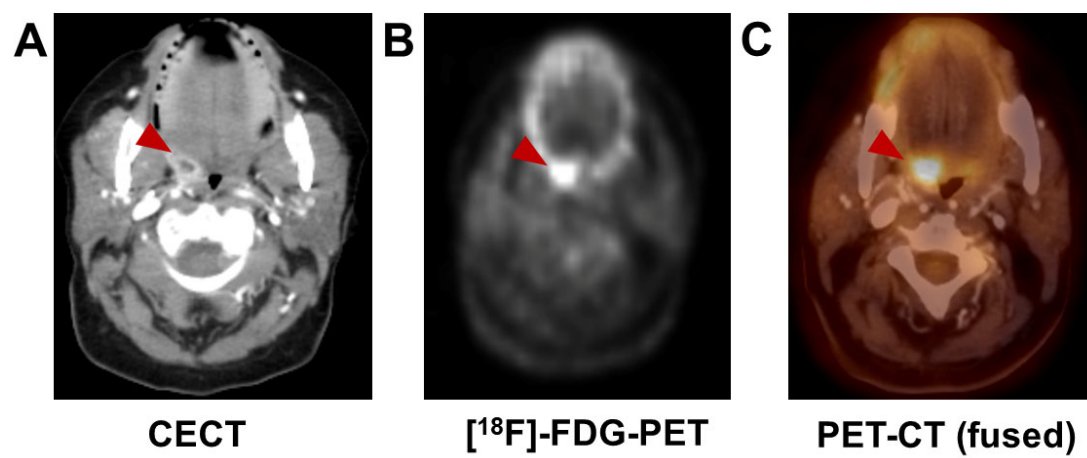


Figure 4: An incidental finding of infection in a 65 y/o female with fallopian tube cancer. (A) Contrast-enhanced CT shows a tonsillar abscess (red arrow); (B+C) focal increase in uptake of FDG in ^{18}F -FDG-PET and ^{18}F -FDG-PET/CT in the same location, respectively.

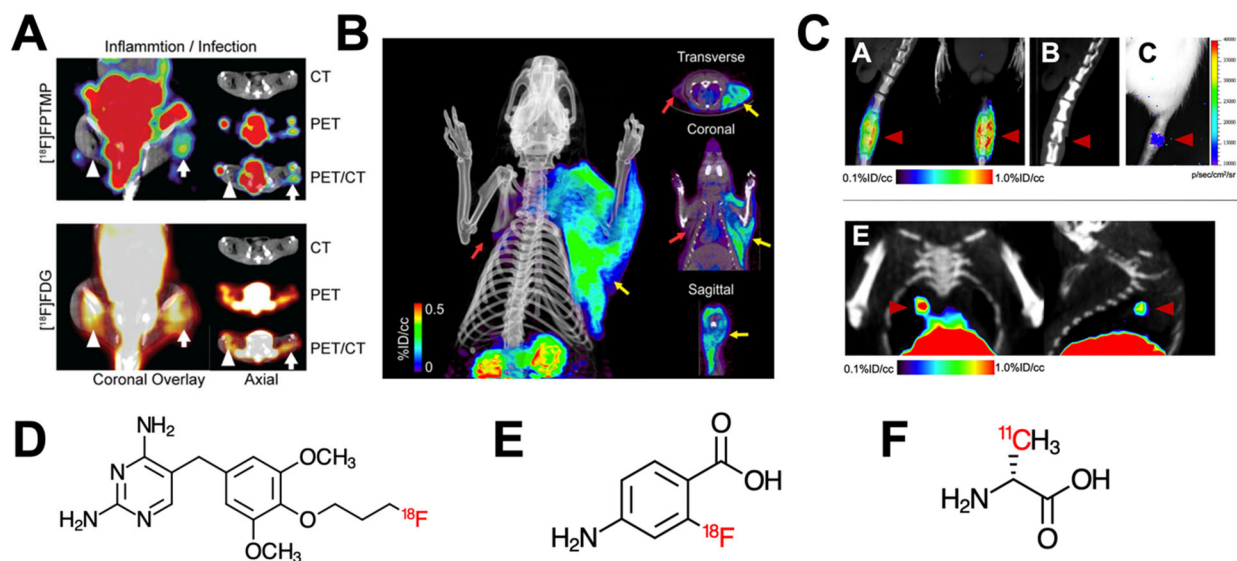


Figure 5: Examples of novel non-sugar-based infection-targeted radiotracers for PET. Images A and B show increased uptake of the radiotracers in infection compared to sterile inflammation in a rodent-models: (A) ^{18}F -FPTMP uptake in mice infected with *E. coli*. From: Sellmyer, M. A. *et al.* (53); (B) ^{18}F -PABA uptake in rat infected with *S. aureus*. From: Zhang, Z. *et al.* (65); (C) ^{11}C -D-Ala uptake in a rat intervertebral disc infected with *S. aureus* and a mouse lung infected with *P. aeruginosa* From: Parker *et al.* (74). Images D to F show the chemical structure of: (D) ^{18}F -FPTMP; (E) ^{18}F -PABA; (F) ^{11}C -D-Ala.

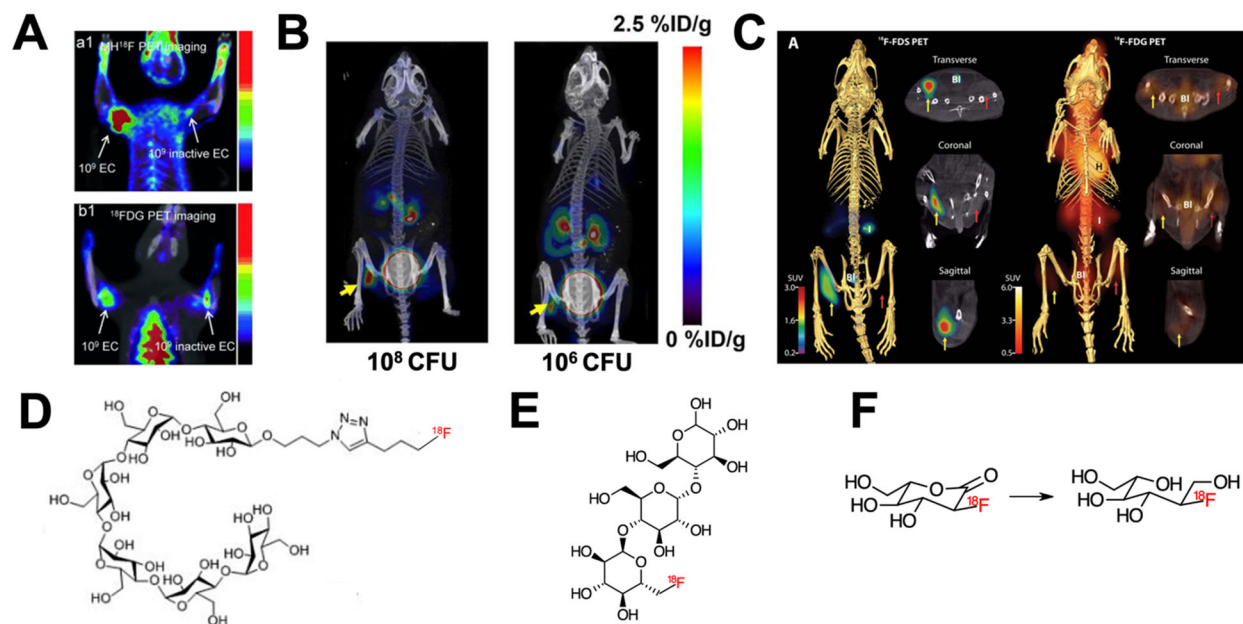


Figure 6: Examples of novel sugar-based infection-targeted radiotracers for PET/CT. Images A to C show increased uptake of the radiotracers in infection compared to sterile inflammation in a rodent-models: (A) ^{18}F -maltohexaose uptake in a rat infected with *E. coli*. From: Ning, X. *et al.* (58); (B) ^{18}F -fluoromaltotriose uptake in mice infected with *E. coli*. From: Gowrishankar, G. *et al.* (60); (C) ^{18}F -FDS uptake in mice infected with *E. coli*. From: Weinstein, E. A. *et al.* (62). Images D to F show the chemical structure of: (D) ^{18}F -maltohexaose; (E) ^{18}F -fluoromaltotriose; (F) ^{18}F -FDS, obtained from chemical reduction of ^{18}F -FDG.

Table 1: Common nuclear imaging techniques (15,76–78)

Radiotracer	Target	Main infectious indications	Half-life	Administered activity (MBq)	Advantages	Disadvantages
Bone scan (^{99m} Tc-MDP)	Active bone formation	PBI* SOM Late PJI Septic arthritis Necrotizing external otitis	6h	500-1,110	Sensitive Low cost Accessible Good spatial resolution Low radiation dose	Low specificity Susceptible to confounders (surgery, trauma etc.)
WBC scan (^{99m} Tc-WBC)	Leukocytes	PBI ** (violated bone) Diabetic foot Early PJI Infective endocarditis Vascular graft infection FUO	6h	185-370	Sensitive, especially for neutrophilic-induced inflammation	Depends on host immune system Sensitivity decreases after antibiotic treatment Blood exposure Requires sterility Time-consuming Poor resolution High radiation dose
⁶⁷ Gallium-citrate	Transferrin Bacterial siderophores Neutrophilic lactoferrin	SOM Opportunistic infections FUO Necrotizing external otitis	78.3h	150-220	Suitable for immunodeficiency	Delayed imaging Poor resolution High radiation dose Expensive Requires cyclotron
¹⁸ F-FDG-PET	Energy consumption	PBI* SOM Infective endocarditis vascular graft infection FUO	110 mins	185-740	Sensitive Suitable for acute and chronic inflammation High resolution Relatively short scan SUV quantification	Depends on host immune system Expensive Lacks widespread availability Susceptible to confounders (surgery, etc.) Requires patient preparation High radiation dose

PBI- Peripheral Bone Infection * Non-violated bone **Violated bone

Table 2: Recent bacteria-specific radiotracers

Tracer	Mechanism	Target bacterial pathogen*	Pathogens tested <i>in vivo</i> (CFUs** administered)	Max infection to inflammation ratio	Stage (published reports)
¹⁸ F-FPTMP	Inhibition of bacterial dihydrofolate reductase	G+,G-	<i>E. coli</i> (10 ⁶ -10 ⁸) <i>S. aureus</i> (10 ⁸) <i>P. aeruginosa</i> (10 ⁷)	~3 (10 ⁸ <i>E. coli</i> CFU)	Preclinical
¹⁸ F-FAG	Bacterial cell wall	G+,G-	<i>E. coli</i> (10 ⁷)	~2	Preclinical
¹⁸ F-Maltohexaose	Maltodextrin transporter	G+,G-	<i>E. coli</i> (10 ⁵ -10 ⁹)	7 (10 ⁹ CFU)	Preclinical
¹⁸ F-Fluoro-maltose	Maltodextrin transporter	G+,G-	<i>E. coli</i> (10 ⁸)	1.3	Preclinical
¹⁸ F-Fluoro-maltotriose	Maltodextrin transporter	G+, G-	<i>E. coli</i> (10 ⁶ -10 ⁸) <i>L. monocytogenes</i> (2x10 ⁵) <i>P. aeruginosa</i> (10 ⁶) <i>S. aureus</i>	3.4 (10 ⁸ <i>E. coli</i> CFU)	Preclinical
¹⁸ F-FDS	Bacterial energy consumption	G-***	<i>E. coli</i> (10 ⁷) <i>S. aureus</i> (10 ⁷ -10 ⁸) <i>P. aeruginosa</i> (10 ^{6.5})	7.3 (<i>E. coli</i>)	Clinical
¹¹ C-PABA	Folic acid biosynthesis	G+,G-	<i>E. coli</i>	2.6	Preclinical
¹⁸ F-PABA	Folic acid biosynthesis	G+,G-	<i>S. aureus</i> (10 ⁷ -10 ⁸)	7.95 (10 ⁸)	Preclinical
¹¹ C-D-Met	Bacterial cell wall	G+,G-	<i>E. coli</i> <i>S. aureus</i>	2	Clinical
¹¹ C-D-Ala	Bacterial cell wall	G+,G-	<i>E. coli</i> (2.5X10 ⁶) <i>S. aureus</i> (5X10 ⁶) <i>P. aeruginosa</i> (2X10 ⁶)	3.5	Preclinical

*G+ Gram positive bacteria, G- Gram negative bacteria **CFU – Colony forming units

****Enterobacteriaceae*